universe

MDPI

Article

A Phenomenological Model of the Magnetic Field Re-Emergence in Magnetars and Discrepancy Between the Kinematic and Characteristic Ages

Rostislav D. Nikandrov [1] and Sergei B. Popov [2,*]

[1] Department of Physics, Lomonosov Moscow State University, 1/2 Leninskie Gory, 119991 Moscow, Russia; rostis192007@gmail.com
[2] Sternberg Astronomical Institute, Lomonosov Moscow State University, Universitetskij pr. 13, 119234 Moscow, Russia
* Correspondence: sergepolar@gmail.com; Tel.: +7-495-9395006

Abstract

Robust age measurements for isolated neutron stars (NSs) are not easily available. That is why the characteristic age $\tau_{\rm ch} = P/2\dot{P}$ is often used as a proxy. Here, P is the spin period of the NS and $\dot{P}$ is the time derivative of P. Additional assumptions related to the initial properties and spin-down evolution are made to derive $\tau_{\rm ch}$. As a result, it is expected that $\tau_{\rm ch}$ is an upper limit for the real age $\tau_{\rm real}$. Recently, Chrimes et al. presented measurements of kinematic ages $\tau_{\rm kin}$ for several magnetars. Surprisingly, for the majority of these sources, $\tau_{\rm kin} > \tau_{\rm ch}$. We present a simple model that includes a realistic approximation for magnetic field decay in magnetars and a simple phenomenological description of field re-emergence following fallback after the birth of an NS. We demonstrate that this simple model can explain the observed relation $\tau_{\rm kin} > \tau_{\rm ch}$ for a realistic set of parameters.

Keywords: neutron stars; magnetic field; magnetars

1. Introduction

Young neutron stars (NSs) manifest themselves as sources with diverse properties that reflect a variety of their initial properties and evolutionary paths [1–3]. In particular, non-trivial behavior can be a result of initial fallback [4] and further magnetic field evolution [5]. The importance of fallback might be specifically important in the case of so-called central compact objects (CCOs) in supernova remnants (SNRs) observed as thermally emitting X-ray sources [6,7]. Even large magnetic fields can be submerged, resulting in the appearance of so-called 'hidden magnetars' [8].

The magnetic field evolution is especially important for magnetars: anomalous X-ray Pulsars (AXPs) and Soft γ-ray Repeaters (SGRs) [9]. Recently, Chrimes et al. [10] used new observations with the *Hubble* Space Telescope and *James Webb* Space Telescope to measure the proper motions of several magnetars. The measurements allowed them to determine the kinematic ages of these objects. Altogether, Chrimes et al. [10] presented kinematic age estimates for nine magnetars. Interestingly, for eight objects in the sample, the kinematic ages, $\tau_{\rm kin}$, were greater than their characteristic ages $\tau_{\rm ch} \equiv P/2\dot{P}$. Here, P is the spin period of an NS and $\dot{P}$ is its first time derivative.

Kinematic ages are based on proper motion measurements and known birthplaces. The latter can be determined by associating the NS with a young stellar cluster or an SNR. Uncertainties in such associations can result in erroneous kinematic ages. If correctly

Check for updates

Academic Editors: Polychronis Koliogiannis and Charalampos Moustakidis

Received: 7 May 2026
Revised: 17 June 2026
Accepted: 18 June 2026
Published: 20 June 2026

Copyright: © 2026 by the authors. Licensee MDPI, Basel, Switzerland. This article is an open access article distributed under the terms and conditions of the Creative Commons Attribution (CC BY) license.

determined, a kinematic age represents the actual age ($\tau_{\rm real}$) of the NS. On the other hand, for the standard evolution according to the magneto-dipole formula with a constant effective external dipolar magnetic field, $\tau_{\rm ch}$ is an upper limit for $\tau_{\rm real}$, as the initial spin period P_0 can be not much smaller than the present-day period. If the magnetic field significantly decays, as is usually assumed in the case of magnetars, we expect $\tau_{\rm ch} \gg \tau_{\rm real}$ even for $P_0 \ll P$.

The inequality $\tau_{\rm ch} < \tau_{\rm real}$ indicates that the effective external dipolar magnetic field, which is responsible for the spin-down, is growing. Potentially, this can occur due to changes (growth) in the angle χ between the spin axis and the magnetic dipole axes [11], or due to the dynamics of the field in the interiors of the NS [2,12,13]. Finally, the external field, which determines the spin-down of the NS, can increase due to re-emergence after an initial episode of the fallback [14–16].

In this paper, we interpret the result by Chrimes et al. [10] in the framework of a re-emerging magnetic field accounting for the field decay. For the rate of re-emergence, we suggest a simple phenomenological model, and for the decay, we follow the approximation suggested for magnetars in [17].

In the next section, we describe our approach. Then, in Section 3, we present our results. This is followed by a discussion. Our conclusions are given in the Section 5.

2. Model

In this study, the spin-down of an NS is calculated following a very basic approach based on a modified spin-down formula:

$$P\dot{P} = \frac{4\pi^2 B^2 R^6}{Ic^3}(k_0 + k_1 \sin^2\chi). \quad (1)$$

Here, $R = 10^6$ cm is the NS radius, $B(t)$ is the surface equatorial magnetic field, and $I = 10^{45}$ g cm^2 is the moment of inertia. The values of the coefficients are taken as: $k_0 = 1$, $k_1 = 1.2$ [18]. The magnetic obliquity angle is assumed to be constant $\chi = 45^\circ$.

As we want to apply a model for the re-emerging magnetic field, we need to specify $B(t)$. The topic of calculation of magnetic field re-emergence is not new, see e.g., refs. [19–21]. More recent studies in the context of CCOs include, e.g., refs. [14,15]. Instead of direct calculations of the external field growth, which can be quite complicated, accounting for the multipolar field structure and interactions between different modes, e.g., ref. [16], we suggest a simple equation, which can potentially represent the field growth due to different reasons, not only re-emergence after a fallback episode (however, below we focus only on this possibility):[1]

$$B(t) = B_{\rm i} + (B_{\rm c}(t) - B_{\rm i}) \times \exp(-t_{\rm cr}/t). \quad (2)$$

Here, $B_{\rm c}(t)$ is the value of the field at the bottom of the crust. Initially, it is equal to the total buried field $B_{\rm max}$. Without field decay, this is the maximum value that can be reached. $B_{\rm i}$ is the initial external field, i.e., this is the field after the fallback episode is over. In our calculations below, we typically assume $B_{\rm i} = 10^9$ G and $B_{\rm max} = 10^{15}$ G, as we are interested in the evolution of magnetars. Finally, $t_{\rm cr}$ is the characteristic time scale of field growth.

To take into account the magnetic field decay, we apply an equation from [17]:

$$B_{\rm c}(t) = B_{\rm max}\frac{\exp(-t/\tau_{\rm Ohm})}{1 + (\tau_{\rm Ohm}/\tau_{\rm Hall})(1 - \exp(-t/\tau_{\rm Ohm})}. \quad (3)$$

Here, $\tau_{\rm Ohm}$ is the Ohmic time scale. $\tau_{\rm Hall}$ is the Hall time scale. In the calculations, we typically assume that $\tau_{\rm Ohm} = 10^6$ yrs and $\tau_{\rm Hall} = 10^4$ yrs for $B_{\rm c}(t = 0) = B_{\rm max}$. The mag-

netic field evolution for several parameter values is shown in Figure 1. In the figure, we also compare our approximation for the field evolution with detailed calculations by [15]. The long-dashed black line represents the results presented in Figure 6 by Viganó & Pons for $B_{\rm max} = 10^{14}$ G. Note that the latter curve does not account for a rapid Hall cascade.

Note that decay is regulated by the value of the decaying field in the crust, $B_{\rm c}$. This narrows the applicability of our model only to the case of the field buried in a fallback. For other models of the growth of the effective field, it is necessary to modify the equations.

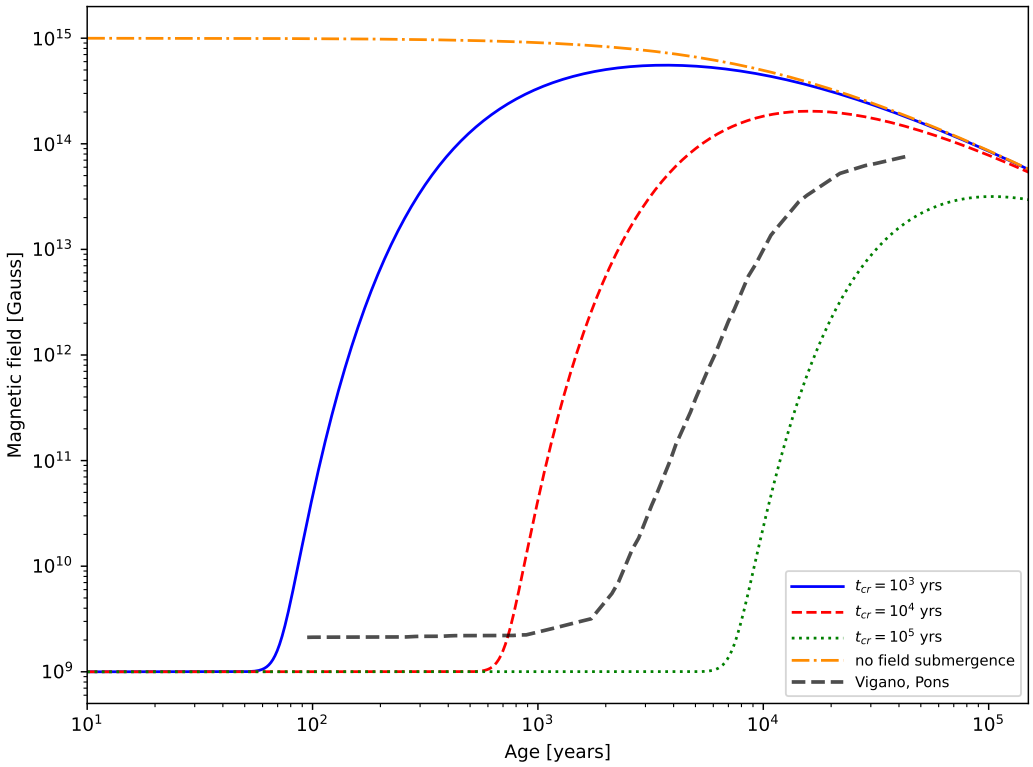


Figure 1. Evolution of the external magnetic field $B(t)$. Blue solid line corresponds to $t_{\rm cr} = 10^3$ yrs, red dashed line to $t_{\rm cr} = 10^4$ yrs, and green dotted line to $t_{\rm cr} = 10^5$ yrs. Orange dash-dotted line represents the model without field submergence for which $B(t) = B_{\rm c}(t)$. Black long-dashed line is digitized from the paper [15].

In our calculations, we do not take into account the Hall attractor [23]. This stage is expected to occur after ≈3 *e*-foldings of the field decay [24]. Substituting this condition into Equation (3), we obtain the characteristic time of transition to the Hall attractor $t_{\rm HA} = 1.7 \times 10^5$ yrs for the initial field $B_{\rm max} = 10^{15}$ G. This value exceeds the typical age of the magnetars under study. But, if we take smaller values of $\tau_{\rm Hall}$, accounting for the Hall attractor becomes necessary. We discuss this in detail in Section 4.

3. Results

In this section, we present the results of our calculations. In all cases, we assume that the initial field before submergence is $B_{\rm max} = 10^{15}$ G and just after submergence is $B_{\rm i} = 10^9$ G. The initial spin period is always taken as $P_0 = 0.1$ s in correspondence with the proposed distributions [25,26] (note that the results do not depend significantly on this value, since $P_0 \ll$ a few seconds). The Hall time scale is taken as 10^4 yrs. We use three values of the field re-emergence time scale $t_{\rm cr}$: 10^3, 10^4, and 10^5 yrs. Note, that such time scales can naturally explain the absence of evolved CCOs among various populations [27]. The middle value approximately corresponds to the calculations in [14,15]. The longest time scale $t_{\rm cr} = 10^5$ yrs is of the order of the time scale obtained in [16] (however, these

authors modeled a pulsar-like field). Obviously, for a smaller amount of fallback matter, the characteristic time scale of re-emergence is shorter. Thus, we also present results for $t_{\rm cr} = 10^3$ yrs and for the absence of the field submergence.

We numerically solve Equation (1), accounting for the field evolution according to Equations (2) and (3). The spin period and period derivative evolution for different values of $t_{\rm cr}$ are presented in the P–$\dot{P}$ diagram (Figure 2).

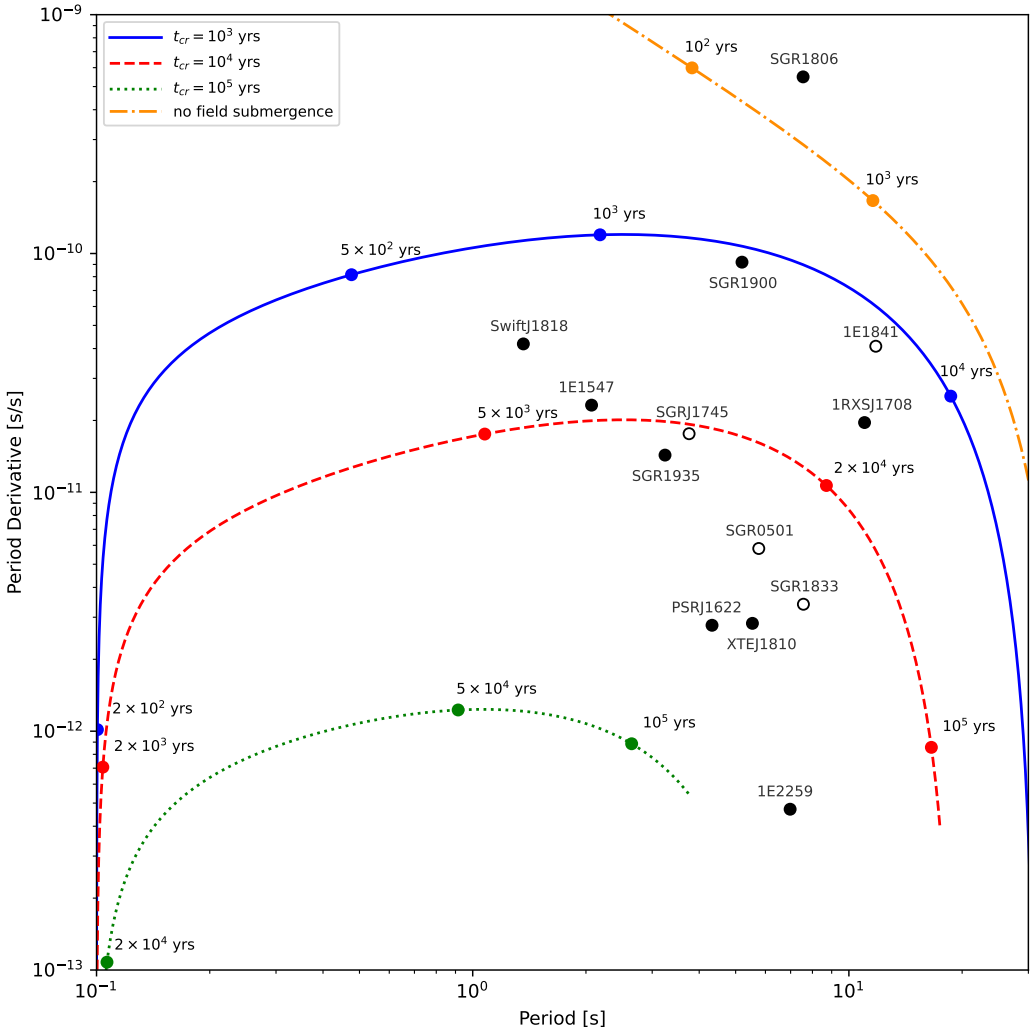


Figure 2. P–$\dot{P}$ diagram. Blue solid line corresponds to $t_{\rm cr} = 10^3$ yrs, red dashed line to $t_{\rm cr} = 10^4$ yrs, green dotted line to $t_{\rm cr} = 10^5$ yrs, and orange dash-dotted line to the model without field submergence. On each curve, we put time-ticks. Data points are taken from the ATNF pulsar catalog [28]. Filled symbols are sources from Chrimes et al. [10], see Table 1. Empty symbols are the sources from Table 2 with unknown kinematic ages.

Each curve for a submerged field starts at $\dot{P} = 2.3 \times 10^{-20}$. The early evolution with rapid growth of $\dot{P}$ is not shown. The curves for $t_{\rm cr} = 10^4$ and 10^5 yrs are truncated at $\approx 1.5 \times 10^5$ yrs before the Hall attractor is reached for the chosen value of $\tau_{\rm Hall}$ (see Section 4). Three stages can be distinguished. In the first brief phase of evolution, $\dot{P}$ and B rapidly grow while P does not increase significantly. Then, the magnetic field continues to increase until the maximum value is reached, and the NS spins down significantly. Finally, the P–$\dot{P}$ evolution is dominated by the field decay.

To illustrate the evolution of an NS during the field re-emergence, we also plot the behavior of the braking index n (Figure 3):

$$n = \frac{\nu\ddot{\nu}}{\dot{\nu}^2} = 2 - \frac{P\ddot{P}}{\dot{P}^2}, \tag{4}$$

where $\nu = 1/P$ is the spin frequency. In this plot, we omit a brief episode when $n \approx 3$ at an early stage of evolution when $B \approx B_i$ (see Section 4).

In the stage of magnetic field re-emergence, the braking index is negative. It rapidly approaches the classical value $n = 3$. In the later stages, the field evolution is dominated by decay. Since decay dominates, the braking index has large positive values. This stage is over when the decay saturates, e.g., when the NS reaches the Hall attractor stage.

Unfortunately, due to the noisy behavior of magnetars, precise measurements of the second spin period derivative are not possible. Still, it is potentially possible to distinguish the sources at the field re-emergence stage by their large negative braking indices. E.g., according to the ATNF catalog [28], several magnetars from the sample we use have large negative braking indices: RXS J170849 and SGR 1806. Several others have large positive braking indices: PSR J1622 has $n = 1.1 \times 10^4$, XTE J1810 has $n = 870$, and SGR 1935 has $n = 5.5 \times 10^3$ (see Table 2 and discussion below).

Our main results are presented in Figure 4. We plot $\tau_{\rm kin}$ vs. $\tau_{\rm ch}$ for nine magnetars from [10], see data in Table 1. For four notable objects (1E 1547, PSR J1622, XTE J1810, and Swift J1818), estimates of $\tau_{\rm ch}$ in [10] and the ATNF catalog are significantly (a factor $\gtrsim$2) different. In such cases, we plot the second point for each of the four sources (see also discussion in Section 4). We overplot four curves based on our model of the magnetic field evolution. Three curves correspond to different values of $t_{\rm cr}$—10^3, 10^4, and 10^5 yrs. The fourth line is plotted for the non-submerged field evolution. To guide an eye, we also show the bisector $\tau_{\rm real} = \tau_{\rm ch}$.

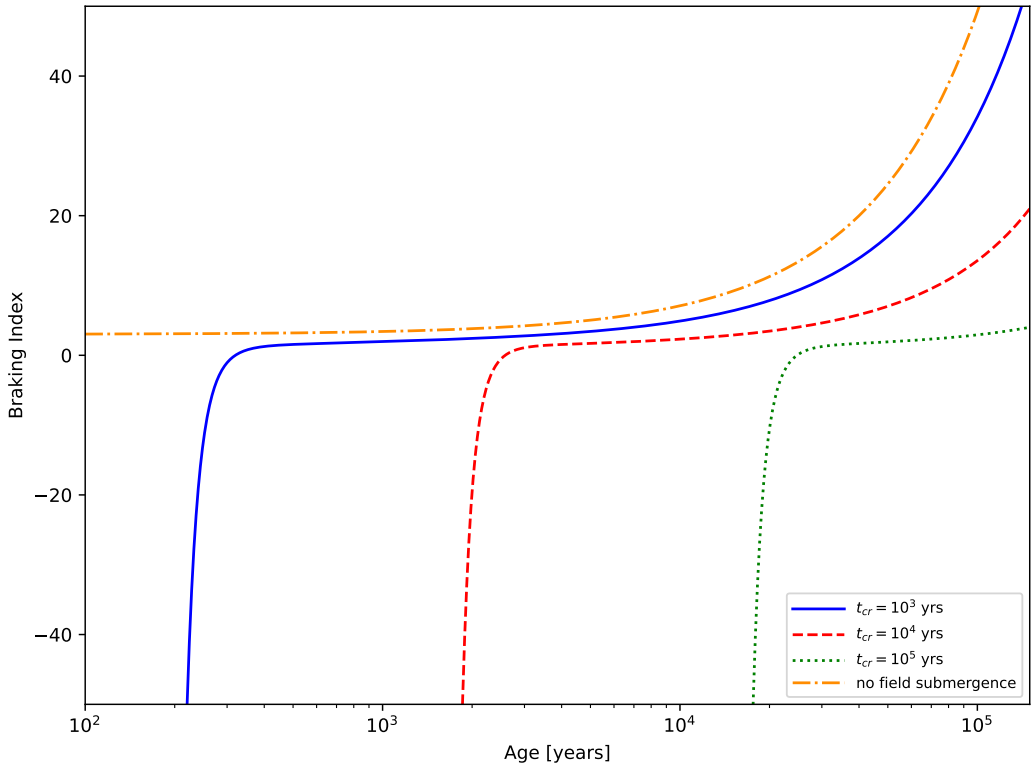


Figure 3. Evolution of the braking index. Blue solid line corresponds to $t_{\rm cr} = 10^3$ yrs, red dashed line to $t_{\rm cr} = 10^4$ yrs, green dotted line to $t_{\rm cr} = 10^5$ yrs, and orange dash-dotted line to the model without field submergence.

The curves for the re-emerging field can be described by three stages (they are also visible in Figure 2, see description above). In the first one (small $\tau_{\rm real}$ and initially large $\tau_{\rm ch}$, which rapidly decreases), the external field is significantly suppressed so that $B(t) \approx B_i$ (compare with Figure 1). At this stage, the evolutionary curve crosses the bisector. In the second stage, the external field rapidly grows and reaches its maximum value. At this stage, $\tau_{\rm real} > \tau_{\rm ch}$. Finally, in the third stage, the field evolution is governed by decay. The curves cross the bisector back. Thus, finally we have $\tau_{\rm real} < \tau_{\rm ch}$.

We see that the curves calculated for the re-emerging field can naturally explain the data points with $\tau_{\rm kin} > \tau_{\rm ch}$ (note that as uncertainties in the birthplace are not included in the kinematic age estimates, for some of the observed sources, the ratio between the two ages can change when more precise data is available). On the other hand, the source AXP 1E 2259 can be explained either by a decaying field alone or by the stage of evolution in which the re-emergence occurred some time ago, with the NS properties regulated mainly by the field decay.

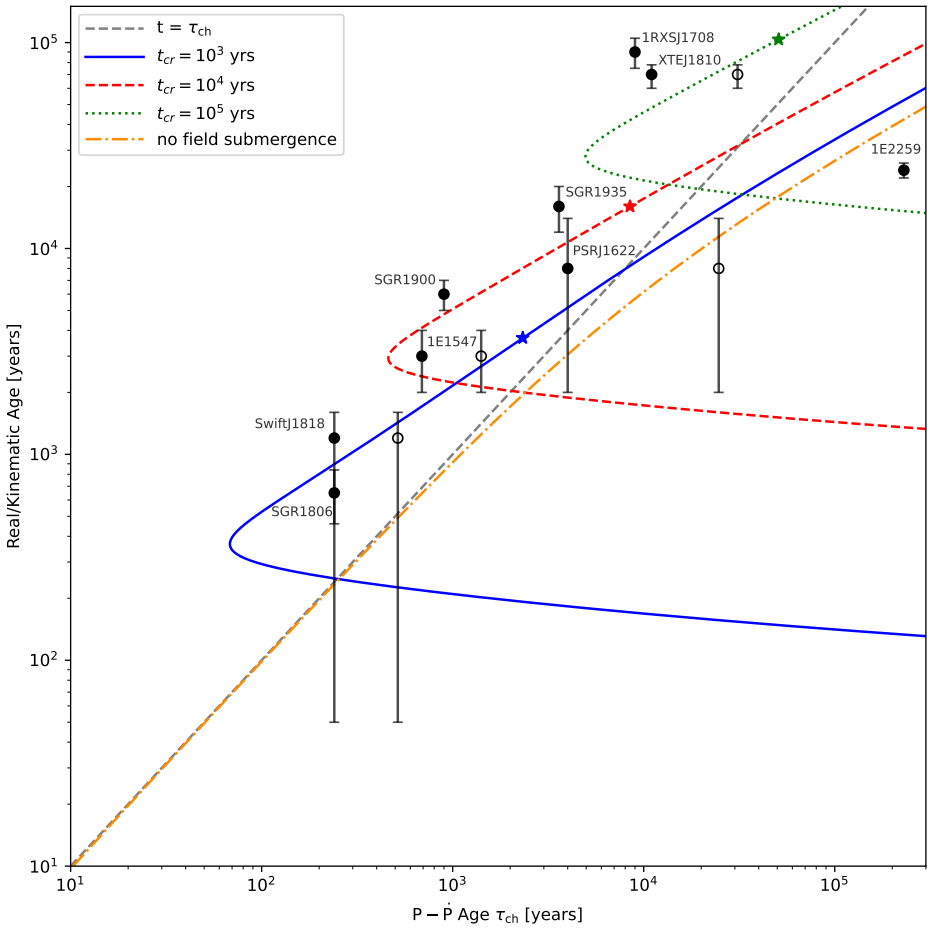


Figure 4. Real/kinematic ages vs. characteristic ages of magnetars. Data points shown with filled black circles are taken from Chrimes et al. [10]. If $\tau_{\rm ch}$ in [10] and ATNF do not match, we add a second point (open symbols) for each such source with $\tau_{\rm ch}$ from the catalog. The colored lines illustrate the evolution of the modeled NSs. Blue solid line corresponds to $t_{\rm cr} = 10^3$ yrs, red dashed line to $t_{\rm cr} = 10^4$ yrs, green dotted line to $t_{\rm cr} = 10^5$ yrs, and orange dash-dotted line to the model without field submergence. On each curve, we mark with a star symbol the moment when the maximum value of the external dipolar field is reached. Grey dashed bisector is plotted for $\tau_{\rm ch} = \tau_{\rm kin}$.

Table 1. Data for magnetars from Figure 4. The values for $\tau_{\rm kin}$ and $\tau_{\rm ch}$ are taken from Chrimes et al. [10]. Periods are taken from ATNF catalog [28]. In cases where the value of $\tau_{\rm ch}$ in Chrimes et al. differs from that in the ATNF catalog, both values are listed (the first being from Chrimes et al.).

Name	P **[s]**	$\tau_{\rm ch}$ **[kyr]**	$\tau_{\rm kin}$ **[kyr]**
SGR 1806-20	7.56	0.24	0.65 ± 0.19
SWIFT J1818.0-1607	1.36	0.24/0.52	$1.20^{+0.40}_{-1.15}$
1E1547.0-5408	2.07	0.69/1.41	3 ± 1
SGR 1900+14	5.20	0.9	6 ± 1
PSR J1622-4950	4.33	4/24.7	8 ± 6
SGR 1935+2154	3.25	3.6	16 ± 4
1E 2259+586	6.98	230	24 ± 2
XTE J1810-197	5.54	11/31	70^{+8}_{-10}
1RXS J170849.0-400910	11.01	9	90 ± 15

Table 2. Magnetars with measured $\ddot{P}$ according to the ATNF catalog.

Name	P **[s]**	$\dot{P}$ **[10^{-12} s/s]**	$\ddot{P}$ **[10^{-21} s/s^2]**	n	$\tau_{\rm ch}$ **[kyr]**	$\tau_{\rm kin}$ **[kyr]**
SGR 1833-0832	7.57	3.4	7.4×10^2	-4.8×10^5	34.9	-
SGR J1745-29	3.76	17.6	1.5×10^3	-1.8×10^4	3.4	-
1E 1841-045	11.79	40.9	54	-380	4.6	-
RXS J170849.0-400910	11.01	19.6	12	-350	8.9	90 ± 15
SGR 1806-20	7.56	549	1.1×10^3	-26	0.22	0.65 ± 0.19
XTE J1810-197	5.54	2.83	-1.3	870	31	70^{+8}_{-10}
SGR 1935+2154	3.25	14.3	-3.5×10^2	5.5×10^3	3.6	16 ± 4
PSR J1622-4950	4.33	2.78	-20	1.1×10^4	24.7	8 ± 6
SGR 0501+4516	5.76	5.82	-2.3×10^2	3.9×10^4	15.7	-

4. Discussion

As our model is not based on detailed calculations of the field diffusion, its applications are limited. In particular, we do not attempt to fit the parameters of individual sources (magnetic field, amount of fallback ΔM, etc.). Some objects can be at the stage of field re-emergence. In others, this stage can be over already, or the fallback is negligible and the field has not been submerged. We ran many simulations with various parameter sets and concluded that, even in our simplified framework, it is possible to fit the individual sources. The results are mostly sensitive to $B_{\rm max}$ and $t_{\rm cr}$. This is illustrated in Figure 5, where we present our results for $B_{\rm max} = 10^{14}$ G and $\tau_{\rm Hall} = 10^5$ yrs. Dependence on B_i, P_0, and $\tau_{\rm Ohm}$ is much smaller. The Hall time is scaled with the magnetic field: $\tau_{\rm Hall} \propto B^{-1}$. Thus, this is not a completely independent parameter. Also, both B_i and $t_{\rm cr}$ might depend on the amount of fallback, ΔM. So, in a more realistic model, there is one parameter fewer. However, in this note, our main goal is to demonstrate that for a natural choice of parameters, it is possible to explain the situation where $\tau_{\rm ch} < \tau_{\rm real}$.

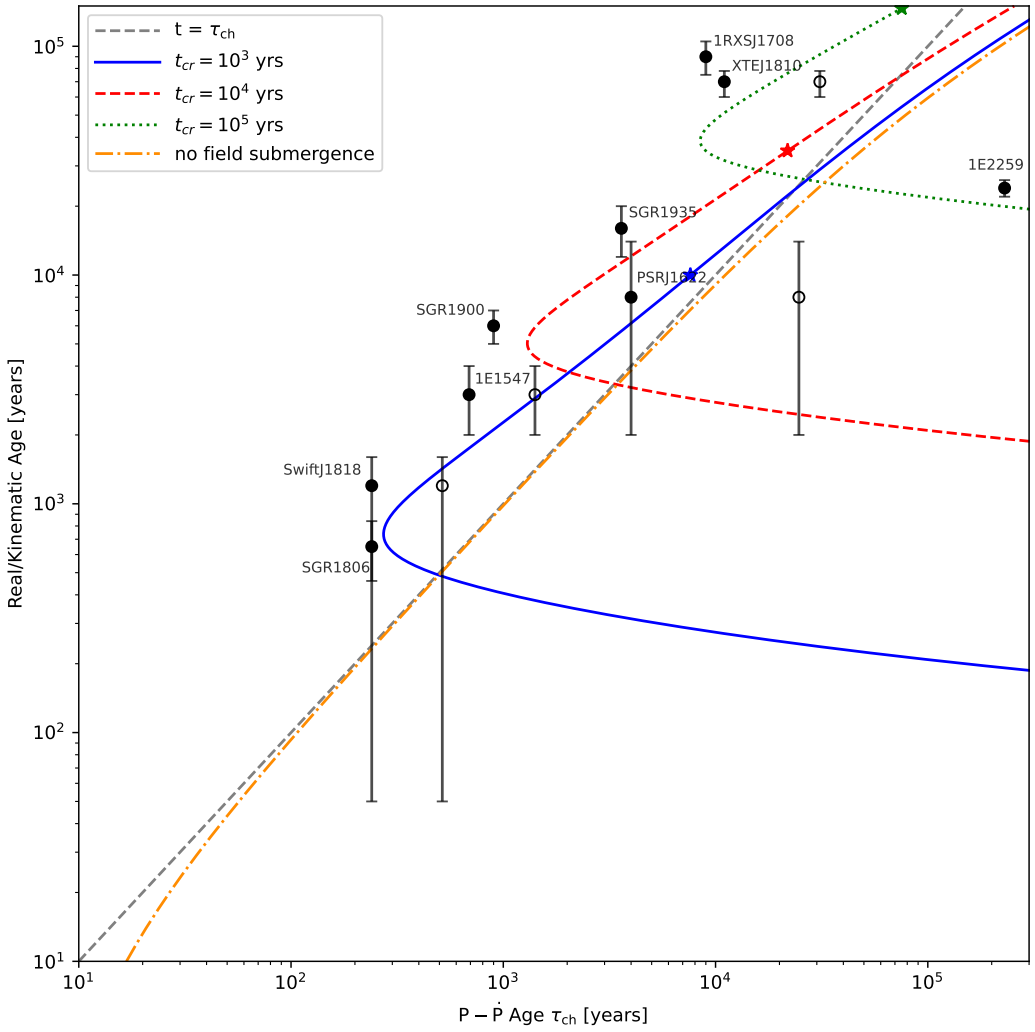


Figure 5. The graph is similar to Figure 4, but for $B_{max} = 10^{14}$ G and $\tau_{Hall} = 10^5$ yrs.

For at least one source in the sample from [10]—AXP 1E 2259—it is observed that $\tau_{ch} > \tau_{real}$. Obviously, this source can be explained naturally without invoking magnetic field re-emergence. However, it is necessary to note that the characteristic ages of magnetars are a subject of significant uncertainty, as the first spin period derivative of these sources is a subject of strong fluctuations. E.g., τ_{ch} of PSR J1622 presented in [10] is taken from the McGill catalog [29]. It is based on $\dot{P}$ measurements from [30]. However, in the ATNF catalog, the period derivative is an order of magnitude smaller [31]. If we use this value, then for PSR J1622, we obtain $\tau_{ch} > \tau_{kin}$ (see Figure 4).

We also face some difficulties in interpreting SGR 1806 as it requires extreme parameters and some fine-tuning. On the one hand, for this source, $\tau_{ch} < \tau_{kin}$, and it has a moderately high negative braking index $n = -25.7$. On the other hand, it has a large magnetic field ($>10^{15}$ G) according to the ATNF catalog [28], which is hard to find in correspondence with the evolution with field submergence and subsequent re-emergence. We speculate that the reason may be related to the application of Equation (1) to calculate the characteristic age. Spin-down of magnetars on the time scale of available observations (i.e., years or tens of years) can significantly deviate from the usual magneto-dipole-like equation due to winds, glitches, anti-glitches, and other factors, e.g., [9,32]. Thus, even accounting for the decaying magnetic field, age estimates based on a momentary application of Equation (1) can provide a wrong value for magnetars. The characteristic age is larger for a given P and $\dot{P}$ if, for the constant field and magnetic obliquity, $n < 3$. E.g., braking

indices < 3 are quite typical for young, well-studied pulsars, see e.g., [33,34]. Otherwise, the second (and maybe the first) derivatives are not precisely known to obtain a correct estimate for τ_{ch} and n. However, the properties of SGR 1806 can be fitted in the framework of the model developed in this note. To do so, it is necessary to assume a large submerged field (B_{max}) and rapid re-emergence. In our framework, the source can be fitted with the following parameters: $B_{max} = 5 \times 10^{15}$ G, $\tau_{Hall} = 2 \times 10^3$ yrs, and $\tau_{cr} = 800$ yrs (all other parameters remain unchanged as they do not influence the results significantly). The large value of the initial magnetic field does not contradict expectations for very young magnetars; however, the observational manifestation of NSs with such large fields in the crust is uncertain, see [35]. However, as we do not intend to fit individual sources in detail, this discussion is beyond the scope of this paper.

Data presented in the ATNF catalog [28] allow for the calculations of braking indices for nine magnetars (SGRs and AXPs). Their parameters are summarized in Table 2 (sources are ordered according to their braking indices). All data except τ_{kin} are taken from the ATNF catalog. The kinematic ages (if known) are taken from [10]. Five of them are presented among the objects with measured τ_{kin} [10]. Three of the remaining four have high negative values of n. However, as the second spin frequency derivative is not well-measured for magnetars, it would be premature to say that these objects are at the stage of magnetic field re-emergence. Sources XTE J1810 and SGR 1935 with positive braking indices can potentially be explained as NSs with initially submerged fields, which are now in the evolutionary stage dominated by decay (see Figure 2).

In our calculations, we neglect the stage of the Hall attractor. As originally proposed in [23,24], this stage can be reached after the dipolar field has decayed by a factor $\sim(e^2$–$e^3)$. In the case of a magnetar-scale initial magnetic field and depending on the value of τ_{Hall}, this can happen in a few $\times 10^3$–10^5 yrs.

We made additional runs of the code, accounting for the Hall attractor stage for the same set of B_{max}, B_i, τ_{Ohm}, and the same three values of t_{cr}. In our calculations, the transition to the Hall attractor happens at t_{HA} when $B_c = B_{max}/20$. As soon as the Hall attractor is reached, the magnetic field in the crust evolves only due to Ohmic dissipation according to the following equation:

$$B_c(t) = B_c(t_{HA}) \times \exp(-(t - t_{HA})/\tau_{Ohm}). \quad (5)$$

For $\tau_{Hall} = 10^4$ yrs, as we mentioned above, the transition to the Hall attractor happens at $t_{HA} = 1.7 \times 10^5$ yrs. Thus, in this case, the inclusion of this stage does not influence our results. If $\tau_{Hall} = 10^3$ yrs, then the transition happens at $t_{HA} = 1.9 \times 10^4$ yrs. This marginally modifies our results, but leaves the main conclusions untouched, as we do not intend to fit all individual sources. Thus, we conclude that as soon as the goal is to explain active magnetars, i.e., the sources which, by definition, did not reach the Hall attractor stage, its inclusion is not necessary. It is necessary only to ensure that the ages of objects in the model do not exceed the transition time for the chosen set of parameters, in particular B_{max}, τ_{Hall}, t_{cr}.

Finally, we have to make a brief comment on the very early behavior of the braking index in our model. In Figure 3, we neglected this stage as objects of interest are older than the duration of this early phase. The early evolution of n, P, $\dot{P}$, and $\ddot{P}$ for $t_{cr} = 10^4$ yrs is shown in Figure 6. Focusing on the early stages, we truncate this plot at $t = 10^4$ yrs. After this time, for the chosen set of parameters, the field evolution is dominated by decay.

https://doi.org/10.3390/universe12060183

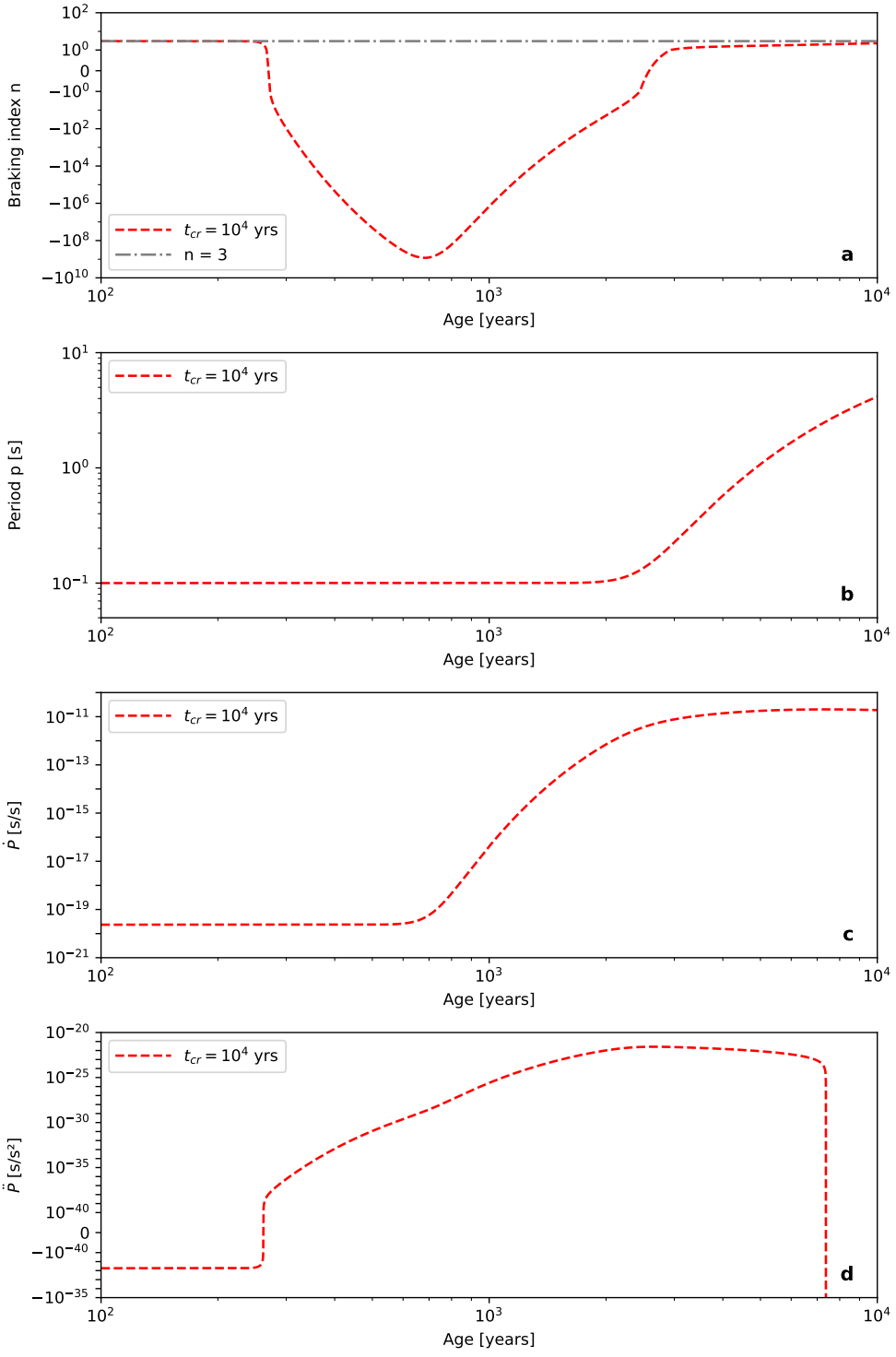


Figure 6. Evolution of the braking index, spin period, period derivative, and the second derivative for $t_{\rm cr} = 10^4$ yrs, $B_{\rm max} = 10^{15}$ G, $\tau_{\rm Hall} = 10^4$ yrs. (**a**): Evolution of n. (**b**): Evolution of P. (**c**): Evolution of $\dot{P}$. (**d**): Evolution of $\ddot{P}$.

The evolution of P and $\dot{P}$ (Figure 6b,c) is rather obvious. At first, while $t \ll t_{\rm cr}$, the period derivative is small as $B(t) \approx B_i$. Then, the period derivative grows as the field starts to re-emerge. Finally, the growth saturates as $\tau_{\rm Hall}$ is of the same value as $t_{\rm cr}$.

The evolution of the braking index and of the second spin period derivative in the early stage $2 \times 10^2 \lesssim t \lesssim 7 \times 10^2$ yrs is less trivial (a and d panels in Figure 6). A rapid 'jump' in n and $\ddot{P}$ and the exact shape of the curves representing the decrease in n and the increase in $\ddot{P}$

are artifacts of the chosen parameterization of the field evolution, i.e., Equations (2) and (3). Thus, this behavior is unphysical. Fortunately, it happens at early ages, which are irrelevant for our discussion.

5. Conclusions

In this study, we presented a simple model of the evolution of magnetars' external magnetic fields, aiming to explain the relation between kinematic and characteristic ages reported by Chrimes et al. [10]. The key ingredient of our model is a simplified one-parameter description of magnetic field re-emergence after an episode of fallback. In our framework, we successfully reproduced $\tau_{\rm kin} > \tau_{\rm ch}$ under the assumption that the magnetic field of some magnetars has been significantly submerged due to fallback. The high negative braking indices reported for several magnetars may indicate that they are still in the stage of field re-emergence.

Author Contributions: Conceptualization, S.B.P.; Methodology, S.B.P.; Software, R.D.N.; Formal analysis, R.D.N. and S.B.P.; Investigation, R.D.N. and S.B.P.; Writing—original draft, S.B.P.; Writing—review & editing, S.B.P.; Visualization, R.D.N.; Supervision, S.B.P.; Funding acquisition, S.B.P. The authors contributed to this study equally. All authors have read and agreed to the published version of the manuscript.

Funding: SP acknowledges support from the RSF grant 25-12-00012.

Data Availability Statement: The code used for modeling is accessible on request. Please, contact the first author.

Acknowledgments: We thank Anton Biryukov and Andrei Igoshev for discussions. We thank anonymous referees for useful comments that helped to improve the manuscript.

Conflicts of Interest: The authors declare no conflicts of interest.

Abbreviations

The following abbreviations are used in this manuscript:

AXP	Anomalous X-ray pulsar
NS	Neutron star
SGR	Soft gamma-ray repeater

Note

[1] A similar approach, but without accounting for the magnetic field decay, was applied by Bernal & Page [22] to explain some properties of CCOs.

References

1. Popov, S.B. The Zoo of Isolated Neutron Stars. *Universe* **2023**, *9*, 273. [CrossRef]
2. Borghese, A.; Esposito, P. Isolated Neutron Stars. In *Handbook of X-Ray and Gamma-Ray Astrophysics*; Springer: Singapore, 2023; p. 146. [CrossRef]
3. Rigoselli, M. X-ray observations of isolated neutron stars. In *Proceedings of the Multifrequency Behaviour of High Energy Cosmic Sources XIV*; SISSA Medialab: Trieste, Italy, 2024; p. 55. [CrossRef]
4. Chevalier, R.A. Neutron Star Accretion in a Supernova. *Astrophys. J.* **1989**, *346*, 847. [CrossRef] [PubMed]
5. Igoshev, A.P.; Popov, S.B.; Hollerbach, R. Evolution of Neutron Star Magnetic Fields. *Universe* **2021**, *7*, 351. [CrossRef]
6. De Luca, A. Central compact objects in supernova remnants. *J. Phys. Conf. Ser.* **2017**, *932*, 012006. [CrossRef]
7. Safi-Harb, S. Neutron stars: Observational diversity and evolution. *J. Phys. Conf. Ser.* **2017**, *932*, 012005. [CrossRef]
8. Shabaltas, N.; Lai, D. The Hidden Magnetic Field of the Young Neutron Star in Kesteven 79. *Astrophys. J.* **2012**, *748*, 148. [CrossRef]
9. Turolla, R.; Zane, S.; Watts, A.L. Magnetars: The physics behind observations. A review. *Rep. Prog. Phys.* **2015**, *78*, 116901. [CrossRef] [PubMed]

10. Chrimes, A.A.; Lyman, J.D.; Levan, A.J.; Borghese, A.; de Bruijne, J.H.J.; Fruchter, A.S.; Guarcello, M.G.; Kouveliotou, C.; Tanvir, N.R.; Wiersema, K. Magnetar counterparts, kinematics and birth sites with HST and JWST. *arXiv* **2026**, arXiv:2603.15750. [CrossRef]
11. Biryukov, A.; Abolmasov, P.; Levinson, A. Rotational Evolution of Deformed Magnetized Neutron Stars: Implications for Obliquity Distribution and Braking Indices Statistics. *Astrophys. J.* **2025**, *995*, 167. [CrossRef]
12. Gourgouliatos, K.N.; Hollerbach, R.; Igoshev, A.P. Powering central compact objects with a tangled crustal magnetic field. *Mon. Not. R. Astron. Soc.* **2020**, *495*, 1692–1699. [CrossRef]
13. Dehman, C.; Brandenburg, A. Reality of inverse cascading in neutron star crusts. AA **2025**, *694*, A39. [CrossRef]
14. Ho, W.C.G. Evolution of a buried magnetic field in the central compact object neutron stars. *Mon. Not. R. Astron. Soc.* **2011**, *414*, 2567–2575. [CrossRef]
15. Viganò, D.; Pons, J.A. Central compact objects and the hidden magnetic field scenario. *Mon. Not. R. Astron. Soc.* **2012**, *425*, 2487–2492. [CrossRef]
16. Igoshev, A.P.; Elfritz, J.G.; Popov, S.B. Post-fall-back evolution of multipolar magnetic fields and radio pulsar activation. *Mon. Not. R. Astron. Soc.* **2016**, *462*, 3689–3702. [CrossRef]
17. Aguilera, D.N.; Pons, J.A.; Miralles, J.A. 2D Cooling of magnetized neutron stars. *Astron. Astrophys.* **2008**, *486*, 255–271. [CrossRef]
18. Philippov, A.; Tchekhovskoy, A.; Li, J.G. Time evolution of pulsar obliquity angle from 3D simulations of magnetospheres. *Mon. Not. R. Astron. Soc.* **2014**, *441*, 1879–1887. [CrossRef]
19. Muslimov, A.; Page, D. Delayed Switch-on of Pulsars. *Astrophys. J. Part 2-Lett.* **1995**, *440*, L77. [CrossRef]
20. Muslimov, A.; Page, D. Magnetic and Spin History of Very Young Pulsars. *Astrophys. J.* **1996**, *458*, 347. [CrossRef] [PubMed]
21. Geppert, U.; Page, D.; Zannias, T. Submergence and re-diffusion of the neutron star magnetic field after the supernova. *Astron. Astrophys.* **1999**, *345*, 847–854.
22. Bernal, C.G.; Page, D. Growing Magnetic Fields in Central Compact Objects. In *Proceedings of the Revista Mexicana de Astronomia y Astrofisica Conference Series*; Revista Mexicana de Astronomia y Astrofisica Conference Series; Instituto de Astronomía, Universidad Nacional Autónoma de México (UNAM): Ciudad de México, Mexico, 2011; Volume 40, pp. 149–150.
23. Gourgouliatos, K.N.; Cumming, A. Hall Attractor in Axially Symmetric Magnetic Fields in Neutron Star Crusts. *Phys. Rev. Lett.* **2014**, *112*, 171101. [CrossRef] [PubMed]
24. Gourgouliatos, K.N.; Cumming, A. Hall effect in neutron star crusts: Evolution, endpoint and dependence on initial conditions. *Mon. Not. R. Astron. Soc.* **2014**, *438*, 1618–1629. [CrossRef]
25. Popov, S.B.; Turolla, R. Initial spin periods of neutron stars in supernova remnants. *Astrophys. Space Sci.* **2012**, *341*, 457–464. [CrossRef]
26. Igoshev, A.P.; Frantsuzova, A.; Gourgouliatos, K.N.; Tsichli, S.; Konstantinou, L.; Popov, S.B. Initial periods and magnetic fields of neutron stars. *Mon. Not. R. Astron. Soc.* **2022**, *514*, 4606–4619. [CrossRef]
27. Popov, S.B.; Turolla, R. Initial Parameters of Neutron Stars. In *Proceedings of the Electromagnetic Radiation from Pulsars and Magnetars*; Lewandowski, W., Maron, O., Kijak, J., Eds.; Astronomical Society of the Pacific Conference Series; ASP: San Francisco, CA, USA, 2012; Volume 466, p. 191. [CrossRef]
28. Manchester, R.N.; Hobbs, G.B.; Teoh, A.; Hobbs, M. The Australia Telescope National Facility Pulsar Catalogue. *Astron. J.* **2005**, *129*, 1993–2006. [CrossRef]
29. Olausen, S.A.; Kaspi, V.M. The McGill Magnetar Catalog. *Astrophys. J. Suppl. Ser.* **2014**, *212*, 6. [CrossRef]
30. Anderson, G.E.; Gaensler, B.M.; Slane, P.O.; Rea, N.; Kaplan, D.L.; Posselt, B.; Levin, L.; Johnston, S.; Murray, S.S.; Brogan, C.L.; et al. Multi-wavelength Observations of the Radio Magnetar PSR J1622-4950 and Discovery of Its Possibly Associated Supernova Remnant. *Astrophys. J.* **2012**, *751*, 53. [CrossRef]
31. Scholz, P.; Camilo, F.; Sarkissian, J.; Reynolds, J.E.; Levin, L.; Bailes, M.; Burgay, M.; Johnston, S.; Kramer, M.; Possenti, A. Spin-Down Evolution and Radio Disappearance of the Magnetar PSR J1622-4950. *Astrophys. J.* **2017**, *841*, 126. [CrossRef]
32. Hamil, O.; Stone, J.R.; Urbanec, M.; Urbancová, G. Braking index of isolated pulsars. *Phys. Rev. D* **2015**, *91*, 063007. [CrossRef]
33. Kaspi, V.M.; Helfand, D.J. Constraining the Birth Events of Neutron Stars. In *Proceedings of the Neutron Stars in Supernova Remnants*; Slane, P.O., Gaensler, B.M., Eds.; Astronomical Society of the Pacific Conference Series; ASP: San Francisco, CA, USA, 2002; Volume 271, p. 3. [CrossRef]
34. Yue, Y.L.; Xu, R.X.; Zhu, W.W. What can the braking indices tell us about the nature of pulsars? *Adv. Space Res.* **2007**, *40*, 1491–1497. [CrossRef]
35. Kojima, Y.; Kisaka, S.; Fujisawa, K. Evolutionary Deformation Toward the Elastic Limit by a Magnetic Field Confined in the Neutron-Star Crust. *Astrophys. J.* **2023**, *946*, 75. [CrossRef]

Disclaimer/Publisher's Note: The statements, opinions and data contained in all publications are solely those of the individual author(s) and contributor(s) and not of MDPI and/or the editor(s). MDPI and/or the editor(s) disclaim responsibility for any injury to people or property resulting from any ideas, methods, instructions or products referred to in the content.